NASA TECHNICAL MEMORANDUM

NASA TM X-67873

NASA TM X-67873

THE SERIES HYBRID BEARING - A NEW HIGH SPEED BEARING CONCEPT

by William J. Anderson, David P. Fleming,
and Richard J. Parker
Lewis Research Center
Cleveland, Ohio

TECHNICAL PAPER proposed for presentation at
Lubrication Conference sponsored by the American
Society of Lubrication Engineers and the American
Society of Mechanical Engineers
Pittsburgh, Pennsylvania, October 5-7, 1971

E-5817

THE SERIES HYBRID BEARING - A NEW HIGH SPEED BEARING CONCEPT

by William J. Anderson,* David P. Fleming,**
and Richard J. Parker†

Lewis Research Center
National Aeronautics and Space Administration
Cleveland, Ohio

ABSTRACT

The series hybrid bearing couples a fluid-film bearing with a rolling-element bearing such that the rolling-element bearing inner race runs at a fraction of shaft speed. A series-hybrid bearing was analyzed and experiments were run at thrust loads from 100 to 300 pounds and speeds from 4000 to 30 000 rpm. Agreement between theoretical and experimental speed sharing was good. The lowest speed ratio (ratio of ball bearing inner-race speed to shaft speed) obtained was 0.67. This corresponds to an approximate reduction in DN value of 1/3. For a ball bearing in a 3 million DN application, fatigue life would theoretically be improved by a factor as great as 8.

INTRODUCTION

Recent developments in gas turbine engines - such as higher thrust-to-weight ratios, advanced compressor design, high temperature materials, and increased power output - have resulted in a requirement

---

*Chief of Bearings Branch, ASME member.
**Head of Fluid Film Bearings Section, ASME member.
†Research engineer, ASME member.

for larger shaft diameters and higher main shaft bearing speeds (ref. 1). Bearings in current production aircraft turbine engines operate in the range from 1.5 to 2 million DN (bearing bore in mm times shaft speed in rpm). Engine designers anticipate that during the next decade turbine bearing DN values will have to increase to the range of 2.5 to 3 million. It is speculated that after 1980 turbine engine developments may require bearing DN values as high as 4 million.

When ball bearings are operated at DN values above 1.5 million, centrifugal forces produced by the balls can become significant. The resulting increase in Hertz stresses at the outer-race ball contacts can seriously shorten bearing fatigue life. The magnitude of the high-speed bearing problem is evident from the curves of figure 1. The solid curves of figure 1 illustrate the effect of DN on the fatigue life of a thrust loaded 150-mm bore ball bearing at two values of thrust load. These curves are based on the analysis of references 2 and 3. An increase in speed from a DN of 1.8 million to 4.2 million results in a reduction in life of 98 percent at 2000 pounds load and 96 percent at 4000 pounds load. These are typical thrust loads which such a bearing would carry in an aircraft turbine engine.

High centrifugal forces are largely responsible for the drastic reduction in predicted fatigue life at high DN values. It is therefore logical to consider methods for reducing the factors that contribute to ball centrifugal loading. These are ball mass, orbital radius, and orbital speed. Theory indicates that reductions in ball mass can be quite effective in extending bearing fatigue life at high speeds. The dashed curves of figure 1, when compared

with the solid curves, illustrate the theoretical improvement in life with a 50 percent reduction in ball weight. At 3 million DN and 4000 pounds thrust load, for example, fatigue life is improved by a factor of 2.5.

Both thin wall spherically hollow and drilled balls have been evaluated in short-time high speed bearing experiments (refs. 4-7). The drilled ball concept (refs. 6 and 7) shows particular promise for high speed applications. None of the hollow ball concepts has, however, been evaluated in extended time fatigue tests.

Since the orbital radius is more or less fixed by bearing design, the only remaining factor contributing to centrifugal loading is orbital speed. For a conventional bearing design this is primarily a function of shaft speed. The series hybrid bearing reduces the ball orbital speed by reducing the speed of the ball bearing inner ring to a fraction of the shaft speed. In effect the DN value that the ball bearing sees is reduced. In the series hybrid bearing, each component bearing carries the full system load but the two bearings share the speed. One element of the fluid-film bearing (fig. 2) rotates at shaft speed. The second element of the fluid-film bearing rotates with the inner race of the ball bearing at a speed less than shaft speed. The outer race of the ball bearing is mounted in the stationary housing. The intermediate member rotates at a speed such that the torques of the fluid-film and ball bearings are equal.

The potential benefits of the series-hybrid bearing are illustrated in figure 3. The curve for the hollow ball bearing was calculated from the 4000 pound curves in figure 1. The curve for the series hybrid bearing was generated from the 4000 pound solid ball curve of figure 1 by comparing the life at each DN value with the life at a 30 percent lower DN.

At 3 million DN with 30-percent speed reduction the series-hybrid bearing improves life 3.2 times, and at 4 million DN the life improvement factor is 5.7. With hollow balls the life improvement factors at these DN values are approximately 2.5 and 4.2. The series-hybrid bearing is considerably more effective than hollow balls. Furthermore, both approaches could conceivably be utilized simultaneously to effect an even more dramatic life improvement. The series hybrid concept does introduce considerable mechanical complexity, but its potential for extreme speed applications makes it worthy of investigation.

The object of this investigation was to analytically and experimentally evaluate the series-hybrid bearing concept. An analysis of a rotating, pressurized, compensated, incompressibly lubricated fluid film thrust bearing was made. Tests were performed with a series hybrid bearing which incorporated a 75-mm bore angular contact ball bearing having the fluid film bearing attached to its inner race. The magnitudes of speed reduction achieved at various loads and speeds were compared with theoretical predictions.

Tests were conducted in a high-speed air turbine driven bearing test rig. Test conditions includes shaft speeds of 4000 to 30 000 rpm, bearing thrust loads from 100 to 300 pounds and a type II tester fluid as the lubricant. The rolling-element bearing was a 115-series ball bearing. These results were reported initially in references 8 and 9.

APPARATUS AND TEST PROCEDURE

The test apparatus is described fully in reference 8. A pneumatic cylinder loaded the bearing through an externally pressurized gas thrust bearing as shown in figure 2. The bearing torque was measured by an unbonded strain-gage force transducer connected to the periphery of the floating test bearing housing. The ball bearing outer-race temperature

was measured with a thermocouple embedded in a copper bead in the test bearing housing. The test bearing was lubricated as shown in figure 2 with a 0.10-inch-diameter jet guiding oil into the shaft. The shaft rotation pumped the oil to the fluid-film bearing. The oil leaving the fluid-film thrust bearing after liftoff flowed to the ball bearing. In addition, the ball bearing was lubricated with an air-oil mist.

Test Bearing

Fluid-film bearing. - The fluid film bearing consisted of a centrifugally pressurized flat face thrust bearing and a small journal bearing to take any radial load that might be present. The analysis used to evaluate fluid-film thrust bearing designs is presented in the section Analysis. The computer program based on the analysis is given in reference 9. The analysis is for an orifice-compensated annular thrust bearing. A line feed and laminar conditions are assumed, and rotational effects are included. The lubricant supply pressure was taken as the pressure that could be developed from centrifugal effects at the radius of the orifices. Because the fluid film bearing was centrifugally pressurized, relative motion between its inner and outer members (fig. 2) did not take place until the rotative speed was high enough to produce a supply pressure sufficient to separate the surfaces under the applied thrust load. The speed at which separation occurs and slip ensues is termed the lift-off speed.

After the first data were taken, the outer member of the fluid-film bearing (fig. 2) was reduced in diameter from 3.35 to 2.80 inches in order to lower the running torque and increase the relative speed of the fluid-film bearing. The journal bearing was also shortened and two small lubricant supply holes were provided for the journal bearing.

Dimensions of the original and modified fluid film bearing designs are given in table I.

Rolling-element bearing. - The rolling-element bearing portion of the series-hybrid bearing is a 115-series deep-groove ball bearing. One shoulder of the outer race was relieved to make the bearing separable. The one-piece, machined, inner-race-located retainer was silver-plated bronze. Bearing specifications are given in reference 8.

Test Procedure

The test shaft was slowly brought up to speed less than 4000 rpm while system temperatures stabilized. When all temperatures stabilized (after about 90 min), conditions were set for the first data point at either 4000 or 5000 rpm. Data were subsequently taken as shaft speed was increased in 1000- to 2000-rpm increments up to 30 000 rpm. Conditions of temperature equilibrium were reached after about 10 to 20 minutes at each speed. Experiments were conducted at thrust loads from 100 to 300 pounds and speeds from 4000 to 30 000 rpm, at a constant oil inlet temperature of 140° F.

ANALYSIS

The bearing analyzed is shown in figure 4. It comprises a thrust bearing and two journal bearings at the inside and outside thrust bearing radii. The journal bearings enter into the analysis only as they contribute additional constant resistances to the throughflow of lubricant and as they add to the bearing torque. Their lengths may be set at zero when they are not present. A circle of orifices is at radius R_c. Alternatively,

the bearing may have capillary restrictors at radius R_c. The number of orifices or capillaries is assumed large enough to constitute a line source of lubricant. The thrust face clearance varies with radius in a stepwise manner as shown. The lubricant is supplied to the orificies at pressure p_s; it leaves the bearing at the reference pressure $p = 0$. Symbols are defined in the Nomenclature.

The starting point of the analysis is the Navier-Stokes equations for incompressible flow (ref. 10). The usual assumptions of laminar flow, rotational symmetry, constant pressure across the film, no body forces acting on the fluid, negligible fluid inertia and small radial velocity relative to circumferential velocity (see ref. 9) are made. (The latter are standard assumptions in lubrication work. See, for example ref. 11, p. 68.) With these assumptions, and after incorporating the continuity equation, the reduced Navier-Stokes equations become, in cylindrical coordinates,

$$-\rho \frac{v_\theta^2}{r} = -\frac{dp}{dr} + \mu \frac{\partial^2 v_r}{\partial z^2} \tag{1a}$$

$$\frac{\partial}{\partial r}\left[\frac{1}{r}\frac{\partial}{\partial r}(r v_\theta)\right] + \frac{\partial^2 v_\theta}{\partial z^2} = 0 \tag{1b}$$

A solution of equation (1b) is

$$v_\theta = r\omega_2 - r(\omega_2 - \omega_1)\frac{z}{h} \tag{2}$$

where z is measured from the lower thrust surface (fig. 4). Equation (2) may be substituted into equation (1a) and the result integrated twice in z. After the boundary conditions $v_r = 0$ at $z = 0$ and $v_r = 0$ at $z = h$ are applied, the result is

$$v_r = \frac{1}{2\mu}\frac{dp}{dr}(z^2 - zh) - \frac{\rho r}{\mu}\left[\frac{\omega_2^2}{2}(z^2 - zh) - \frac{\omega_2(\omega_2 - \omega_1)}{3h}(z^3 - zh^2) + \frac{(\omega_2 - \omega_1)^2}{12h^3}(z^4 - zh^3)\right] \tag{3}$$

Lurbicant Flow Rates

The quantity of lubricant flowing radially at any radius r is found from

$$Q = 2\pi r \int_0^h v_r \, dz \tag{4}$$

Substituting equation (3) into equation (4) and integrating yield

$$Q = \frac{\pi r h^3}{6\mu}\left(-\frac{dp}{dr} + \rho r \omega_o^2\right) \tag{5}$$

where ω_o is defined by

$$\omega_o^2 = \omega_1\omega_2 + \frac{3}{10}(\omega_2 - \omega_1)^2 \tag{6}$$

The speed ω_o, which may be regarded as an average of ω_1 and ω_2, is used to calculate rotational effects. Equation (5) may now be integrated with respect to r to find the relation between flow and pressure. The clearance h has been assumed to vary in a stepwise manner. Thus,

integration over any interval of constant clearance is straightforward. For example, integrating from $r = R_{po}$ to $r = R \leq R_o$ gives

$$p_{po} - p = -\frac{6\mu Q_o}{\pi h_o^3} \ln \frac{R_{po}}{R} + \frac{\rho}{2}(R_{po}^2 - R^2)\omega_o^2 \tag{7}$$

Pressure drop through the journal bearings is easily calculated from the expression for flow in a narrow slot (ref. 11, p. 99). For the outer journal bearing, neglecting the effect of eccentricity,

$$p_o - p_{ref} = \frac{6\pi Q_o L_o}{\pi R_o C_o^3} \tag{8}$$

With this, total lubricant flow through the bearing can now be given as that flowing inward from the orifices and that flowing outward:

$$Q = Q_o - Q_i = \frac{\pi}{6\mu} \frac{p_c - \frac{\rho}{2}(R_c^2 - R_o^2)\omega_o^2}{\frac{L_o}{R_o C_o^3} + \frac{1}{h_p^3} \ln \frac{R_{po}}{R_c} + \frac{1}{h_o^3} \ln \frac{R_o}{R_{po}}}$$

$$+ \frac{\pi}{6\mu} \frac{p_c - \frac{\rho}{2}(R_c^2 - R_i^2)\omega_o^2}{\frac{L_i}{R_i C_i^3} + \frac{1}{h_p^3} \ln \frac{R_c}{R_{pi}} + \frac{1}{h_i^3} \ln \frac{R_{pi}}{R_i}} \tag{9}$$

The negative of Q_i is taken because, at any radius, outward flow is defined as positive.

The total flow Q must now be matched to the flow through the restrictors. For orifice restrictors, this is (ref. 11, p. 103)

$$Q = C_d n\pi \frac{d^2}{4} \left(\frac{2(p_s - p_c)}{\rho} \right)^{1/2} \tag{10}$$

Equation (10) may be combined with equation (9), and the pressure p_c downstream of the restrictors solved for algebraically. The flow rate Q can then be found from equation (9).

Bearing Loads

The thrust bearing load is given by

$$W = 2\pi \int_{R_i}^{R_o} pr \, dr \tag{11}$$

The pressure p is given by equation (7) for $R_{po} \leq r \leq R_o$, and by similar expressions for other radii. These expressions may be substituted into equation (11) and integrated to yield the load. Inner and outer journal bearings (fig. 4) may be used to provide a radial load capacity. These are assumed to be purely self-acting bearings. For small length-to-diameter ratios, the load is adequately given by the short bearing approximation. From reference 11 (p. 84), for the inner bearing,

$$W_{ji} = \frac{\mu R_i |\omega_1 - \omega_2| L_i^3}{4C_i^2} \frac{\epsilon_i}{\left(1 - \epsilon_i^2\right)^2} \left[\pi^2 (1 - \epsilon_i^2) + 16\epsilon_i^2 \right]^{1/2} \tag{12}$$

where ϵ_i is the journal-bearing eccentricity ratio.

Bearing Torque

The velocity v_θ varies linearly across the film (eq. (2)). Thus, thrust bearing torque is easily calculated. For the annulus from $r = R_c$ to $r = R_{po}$,

$$T_{po} = \frac{\pi\mu\left|\omega_1 - \omega_2\right|(R_{po}^4 - R_c^4)}{2h_p} \tag{13}$$

Similar expressions apply to the other sections. For the inner journal bearing, neglecting the effect of eccentricity, the torque is

$$T_{ji} = \frac{2\pi R_i^3 L_i \mu\left|\omega_1 - \omega_2\right|}{C_i} \tag{14}$$

A similar expression applies to the outer journal bearing. Total torque is merely the sum of the various component torques:

$$T = T_o + T_{po} + T_{pi} + T_i + T_{jo} + T_{ji} \tag{15}$$

Though the preceding analysis is simple and straightforward, a considerable effort would be needed to calculate the large number of numerical results needed in evaluating several bearing designs and operating conditions. To reduce this effort, a computer program was written. It is presented in reference 9.

RESULTS

Original Fluid Film Bearing Design

Ball-bearing inner-race speed is plotted in figure 5 as a function of shaft speed for thrust loads of 100 and 300 pounds. For each load, the

inner race initially rotates at the shaft speed. As shaft speed increases, a point is reached where the fluid-film bearing lifts off. These liftoff points are seen in figure 5 where the data indicate inner-race speed and shaft speed are no longer equal.

As thrust load increases, the liftoff speed increases as shown in figure 6. In this figure, the speed ratio N_i/N_s is plotted against shaft speed (N_i is inner-race speed and N_s is shaft speed) for four thrust loads. The trend of higher liftoff speed with higher thrust load is expected since the load capacity of the fluid-film bearing depends on the lubricant supply pressure. This pressure increases as the square of the shaft speed. Thus, for higher thrust loads, greater hydrostatic pressures (and thus higher shaft speeds) are required for liftoff.

Also shown in figure 6 is the variation in speed ratio N_i/N_s as shaft speed increases beyond the liftoff range. The speed ratio drops rapidly after liftoff but in all cases reaches a minimum value and then begins to increase. Minimum speed ratios were in the range of 0.76 to 0.80. For example, with a shaft speed of 18 000 rpm, the inner-race speed is about 14 000 rpm. Or, in terms of speed sharing, the ball bearing is rotating at 14 000 rpm, and the effective fluid-film bearing speed is 4000 rpm. This speed of 4000 rpm appears to be an upper limit for this fluid-film bearing, concevably because of turbulence in the fluid film. Turbulence can increase the drag of the fluid-film bearing (refs. 12 and 13).

In the tests at 200- and 300-pound thrust loads, the fluid-film bearing ceased to operate when the shaft speed reached 22 000 rpm. At this point, the ball-bearing inner-race speed increased to the shaft speed. This effect

was accompanied by an oscillation in bearing torque which indicated a possible critical speed of the shaft assembly. (This oscillation was also noted at 22 000 rpm in later tests with a modified bearing.) After testing, the bearing was disassembled, and a slight scuffing of the journal bearing surface was noted which could have been a result of this operating condition.

Modified Fluid Film Bearing Design

The fluid-film bearing was modified in an attempt to reduce its torque-to-load-capacity ratio and thus to achieve more favorable speed sharing. The modification consisted of a smaller diameter thrust bearing, a shorter journal bearing length, and lubricant feed holes for the journal bearing. This modified bearing proved to be superior to the initial design in speed sharing capabilities when tested in the same range of test conditions. The results are shown in figure 7. Ratios of ball-bearing inner-race speed to shaft speed as low as 0.67 were obtained, and the speed of the ball bearing was reduced nearly 6000 rpm below the shaft speed at one point. (With the original series-hybrid bearing, the maximum speed reduction was 4000 rpm.)

Liftoff speeds were higher with the modified bearing because of a smaller load-carrying area. Maximum speeds obtained, however, were greater, with the modified bearing still functioning at 30 000 rpm and 300 pounds thrust load (fig. 7).

Torque results for the modified bearing as a function of inner-race speed are shown in figure 8. When the fluid-film bearing lifts off, an abrupt increase in torque occurs because the lubricant leaving the fluid-film thrust bearing also passes through the ball bearing. This increased flow through the ball bearing results in increased torque due to oil drag.

Better speed sharing resulted with the modified fluid film bearing design because it exhibited lower torque at a given relative speed than the original design.

Comparison of Theoretical and Experimental Results

Figures 9 and 10 show the bearing inner-race speed plotted against shaft speed for the original and modified bearings, respectively. The theoretical curves (from the analysis, and the computer program of ref. 9) were calculated from the measured bearing torque and an oil viscosity corresponding to the measured ball-bearing outer-race temperature.

When the liftoff speed is reached, according to the analysis, the inner-race speed drops abruptly. Inner-race speed varies little with applied load, but is sensitive to lubricant viscosity. The 300-pound curve lies below the 100-pound curve in figure 10 since the oil was hotter (hence, less viscous) during the 300-pound run. For the experimental data in figure 9, temperatures did not vary as widely with applied load. A mean temperature was used in these calculations.

Experimental liftoff speeds and inner-race speeds are higher than predicted by theory. Also, the experimental points indicate a nearly constant difference between shaft speed and inner-race speed, whereas the analysis shows the difference increasing with shaft speed. Agreement between theory and experiment is better for the original series-hybrid bearing than for the modified bearing, though, as expected, inner-race speeds are lower for the modified bearing. Higher experimental thrust loads generally resulted in lower inner-race speeds, showing the effect of higher temperatures on the fluid-film bearing.

Possible reasons for the disparity between analysis and experiment are the following:

(1) The analysis assumes a line source of pressurized lubricant, whereas the actual bearing has only four orifices.

(2) The fluid-film bearing may be cooler than the ball-bearing outer race.

(3) There may be some turbulence in the fluid film at higher speeds. The highest Reynolds number, based on the clearance in the bearing recess, was 1240. Reference 14 gives a critical Reynolds number of 1000 for thrust bearings.

CONCLUSIONS

The following results were obtained from the analytical-experimental evaluation of a series hybrid bearing:

1. Reductions in ball bearing speed of up to 33 percent of shaft speed were obtained. This corresponds to a reduction in DN value of 1/3.

2. Experimental values of speed ratio (ratio of ball bearing to shaft speed) were greater than theoretical predictions. Deviation of experimental from predicted speed ratios was greatest at higher speeds.

3. Experimental liftoff speeds increased with increased thrust load and were only slightly higher than theoretical predictions.

These results have several implications regarding improvements in ball-bearing fatigue life. A reduction in ball bearing speed of 33 percent in a 3 million DN application could result in a theoretical life improvement of 8. At higher DN values the life improvement factors would be even more dramatic.

The fluid-film bearing limits the ball bearing speed reduction, and thus the life improvement factor, because it is inherently a higher torque bearing than is a ball bearing. The basic design problem is to devise a fluid film bearing that has the lowest torque at a given load and speed consistent with reasonable lubricant flow requirements. An important advantage of the series hybrid bearing is that its power loss (neglecting the power required to supply the lubricant) will be somewhat less than that of the ball bearing operating at full shaft speed.

NOMENCLATURE

C_d	orifice discharge coefficient
C_i	radial clearance in inner journal bearing, in.
C_o	radial clearance in outer journal bearing, in.
d	orifice diameter, in.
h	thrust bearing clearance, in.
L	journal bearing length, in.
N	speed, rpm
n	number of restrictors
p	pressure, lb/in.^{2}
Q	lubricant flow rate, in.^{3}/sec
R	radius, in.
Re	film rotation Reynolds number, $R\omega h_\rho/\mu$
r	radial coordinate, in.
T	bearing torque, in.-lb
v	velocity, in./sec
W	bearing load, lb
z	axial coordinate, in.
ϵ	journal bearing eccentricity ratio
μ	lubricant dynamic viscosity, lb-sec/in.^{2}
ρ	lubricant density, lb sec^2/in.^{4}
ω	angular velocity, rpm or rad/sec
ω_o	mean angular velocity, eq. (6), rpm or rad/sec

Subscripts:

c	restrictor exit
i	inner, inner race
j	journal bearing
o	outer
p	pocket
r	radial direction
s	supply, shaft
θ	circumferential direction
1	upper thrust surface
2	lower thrust surface

REFERENCES

1. Harris, T. A. "On the Effectiveness of Hollow Balls in High-Speed Thrust Bearings," ASLE Transactions, Vol. 11, no. 4, Oct. 1968, pp. 290-294. Discussion by P. F. Brown, ASLE Transactions, Vol. 12, No. 3, July 1969, pp. 204-205.

2. Althouse, R. C., and Harris, T. A., "Analytical Evaluation of Performance of a 75-mm Bore Thrust-Loaded, Angular Contact Ball Bearing," NASA CR 72692, 1970, SKF Industries, Inc. King of Prussia, Pennsylvania.

3. Harris, T. A., "An Analytical Method to Predict Skidding in Thrust-Loaded, Angular Contact Ball Bearings," Journal of Lubrication Technology, Trans. ASME, Series F. Vol. 93, No. 1, January 1971, pp. 17-24.

4. Coe, H. H., Parker, R. J., and Scibbe, H. W., "Evaluation of Electron-Beam Welded Hollow Balls for High-Speed Ball Bearings," Journal of Lubrication Technology, Trans. ASME, Series F. Vol. 93, No. 1, Jan. 1971, pp. 47-59.

5. Coe, H. H., Scibbe, H. W., and Parker, R. J., "Performance of 75-Millimeter-Bore-Bearings to 1.8 Million DN With Electron-Beam-Welded Hollow Balls," NASA TN D-5800, 1970.

6. Coe, H. H., Scibbe, H. W., and Anderson, W. J., "Evaluation of Cylindrically Hollow (Drilled) Balls in Ball Bearings at DN Values to 2.1 Million," NASA TN D-7007, 1970.

7. Scibbe, H. W. and Zaretsky, E. V., "Advanced Design Concepts for High Speed Bearings," ASME, Paper 71-DE-50, Apr. 1971. New York, N.Y.

8. Parker, R. J., Fleming, D. P., Anderson, W. J., and Coe, H. H., "Experimental Evaluation of the Series-Hybrid Rolling-Element Bearing," NASA TN D-7011, 1970.

9. Fleming, D. P., "Analysis and Computer Program for Evaluation of Rotating Incompressibly Lubricated Pressurized Thrust Bearings," NASA TN D-6075, 1971.

10. Schlichting, H., Boundary Layer Theory, 4th ed., McGraw-Hill, New York, 1962, pp. 53-54.

11. Bisson, E. E., and Anderson, W. J., "Advanced Bearing Technology," NASA SP-38, 1964.

12. Wilcock, D. F., "Turbulence of High Speed Journal Bearings," Transactions ASME, Vol. 72, 1950, pp. 825-834.

13. Smith, M. I., and Fuller, D. D., "Journal-Bearing Operation at Super-laminar Speeds," Transactions ASME, Vol. 78, No. 3, Apr. 1956, pp. 469-474.

14. Constantinescu, V. N., "Theory of Turbulent Lubrication," Proceedings of International Symposium on Lubrication and Wear, D. Muster and B. Sternlicht, eds., McCutchan Publ. Corp., 1965, p. 161.

TABLE I. - FLUID-FILM BEARING SPECIFICATIONS

	Original design	Modified design
Thrust bearing outside diameter, in.	3.35	2.80
Thrust bearing inside diameter, in.	1.75	1.75
Outer recess diamter, in.	2.75	2.60
Inner recess diameter, in.	1.75	1.75
Recess depth, in.	.009	.009
Number of orifices	4	4
Orifice diameter, in.	.010	.010
Orifice locating diameter, in.	2.4	2.4
Journal bearing diameter, in.	1.75	1.75
Journal bearing diametral clearance, in.	.002	.002
Journal bearing length, in.	.86	.61

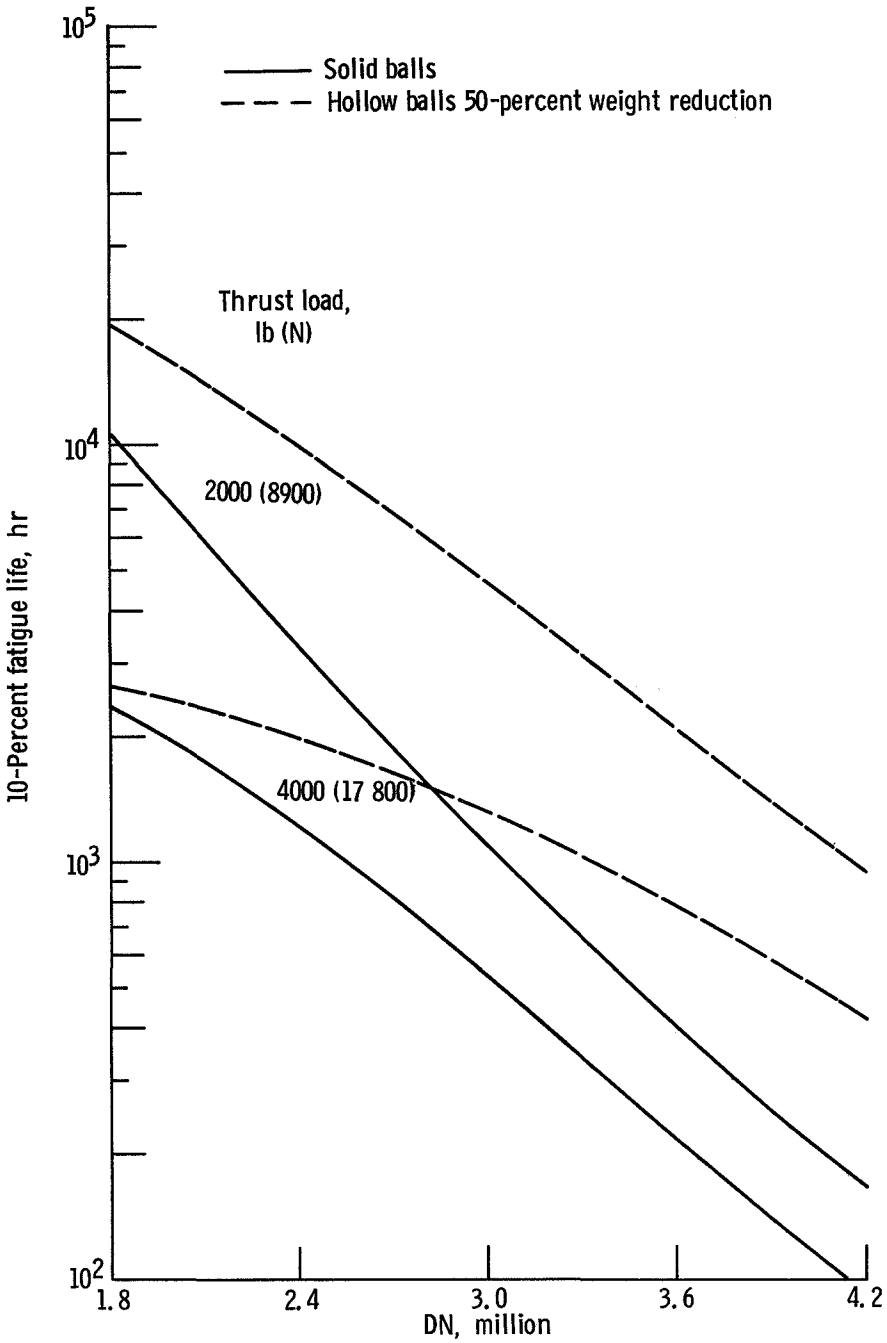

Figure 1. - Theoretical fatigue life of a thrust-loaded 150-mm bore ball bearing with solid and with 50-percent hollow balls (based on analysis of refs. 2 and 3).

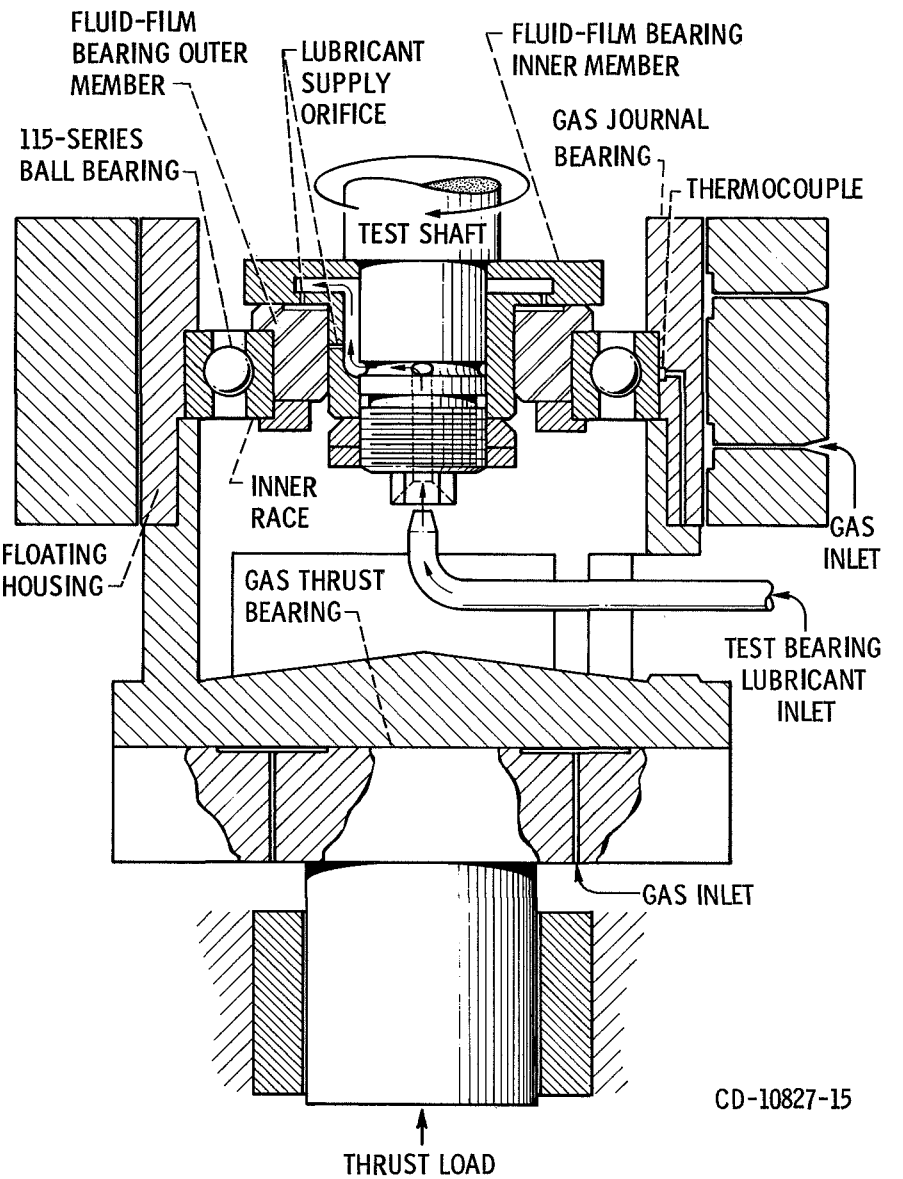

Figure 2. - Cross section of series-hybrid bearing installation.

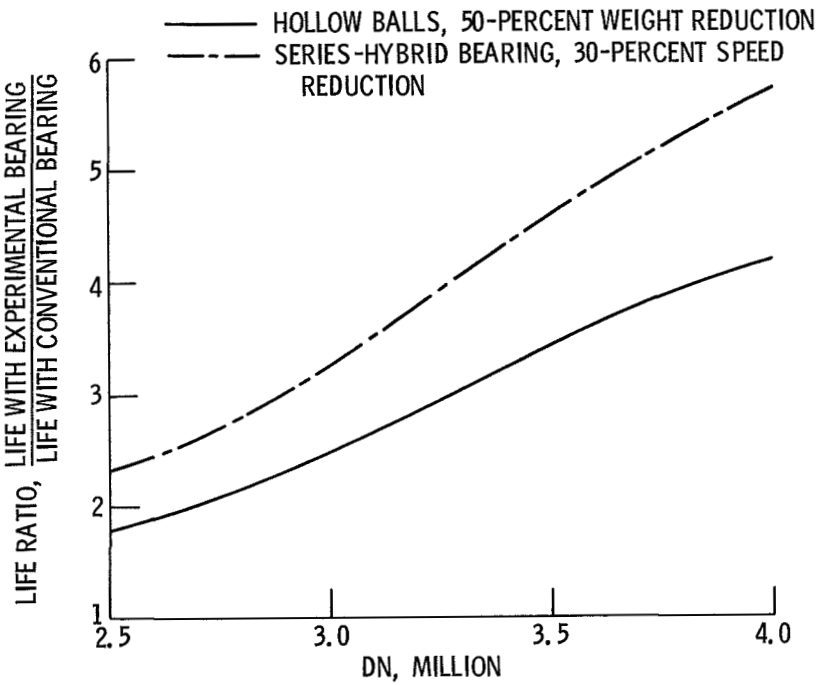

Figure 3. - Theoretical life improvement factors as function of DN for a 150-mm bore ball bearing with hollow balls, and a series-hybrid bearing. Thrust load, 4000 pounds.

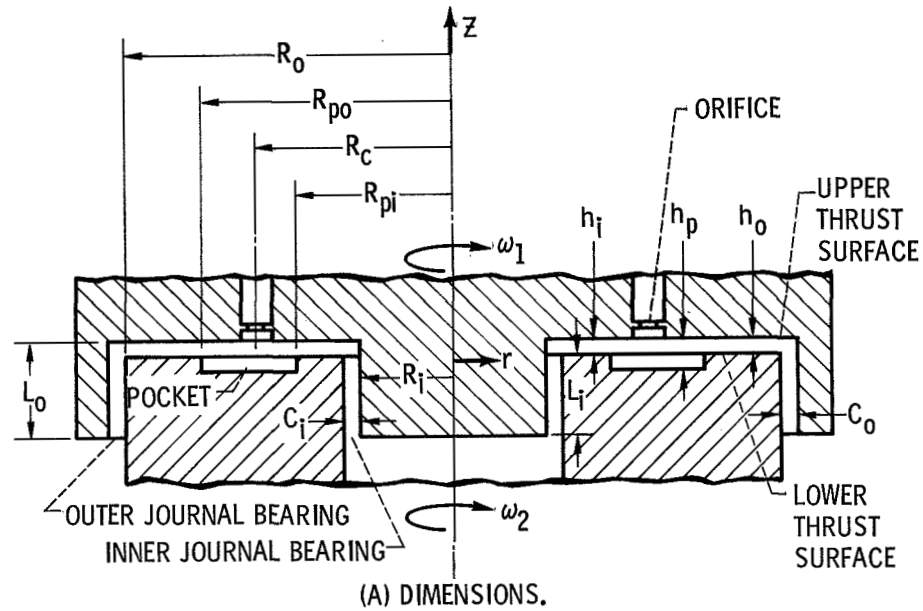

(A) DIMENSIONS.

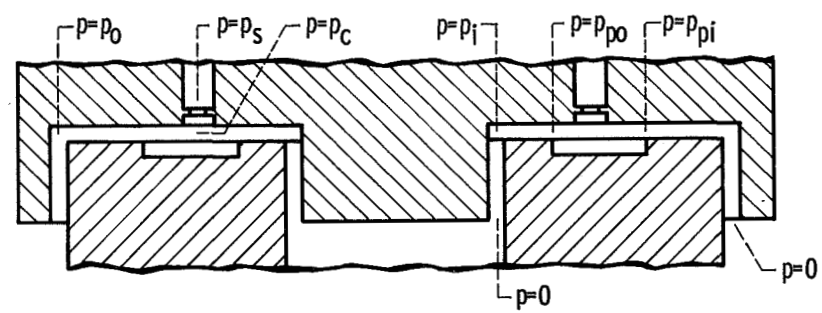

(B) PRESSURES.

Figure 4. - Pressurized thrust bearing.

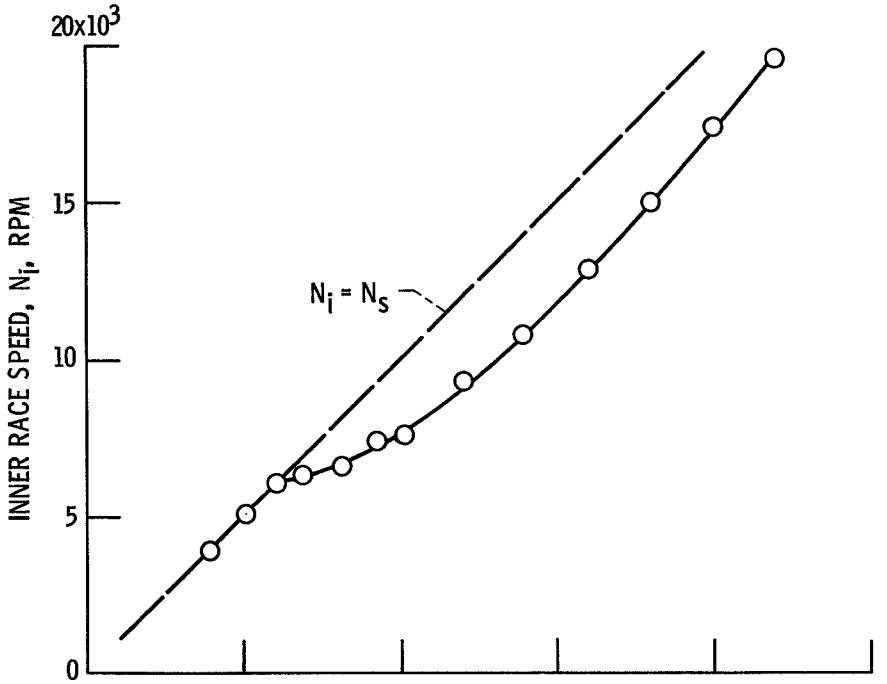

(A) THRUST LOAD, 100 POUNDS.

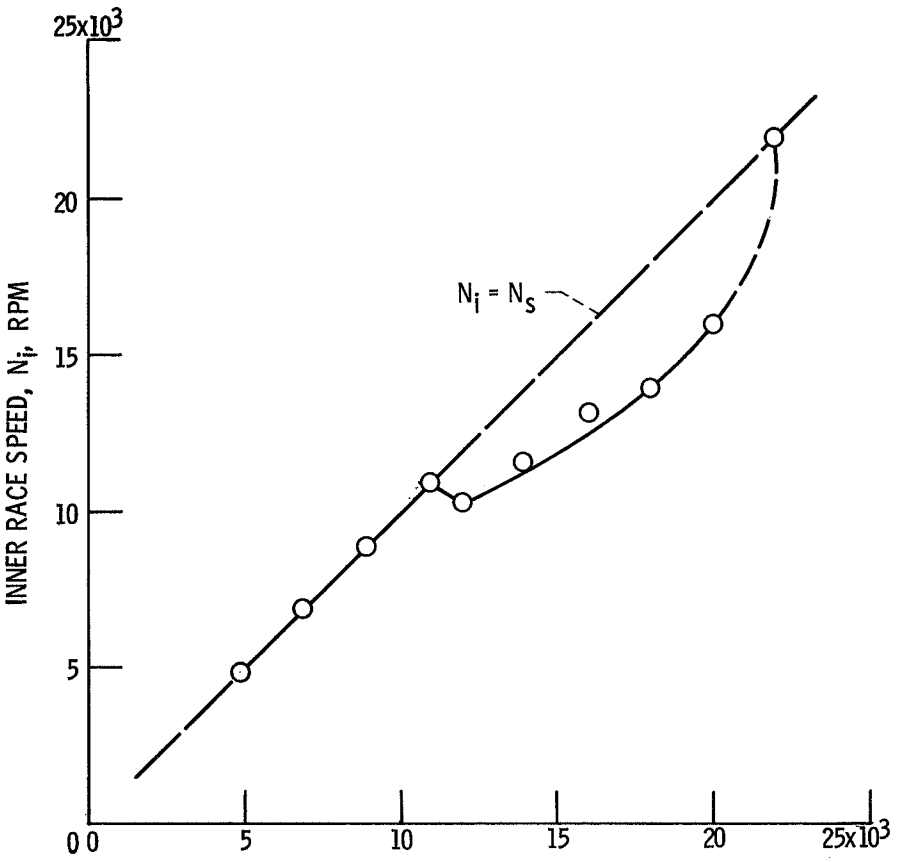

(B) SHAFT SPEED, N_S, RPM

Figure 5. - Inner-race speed as function of shaft speed for original series-hybrid bearing.

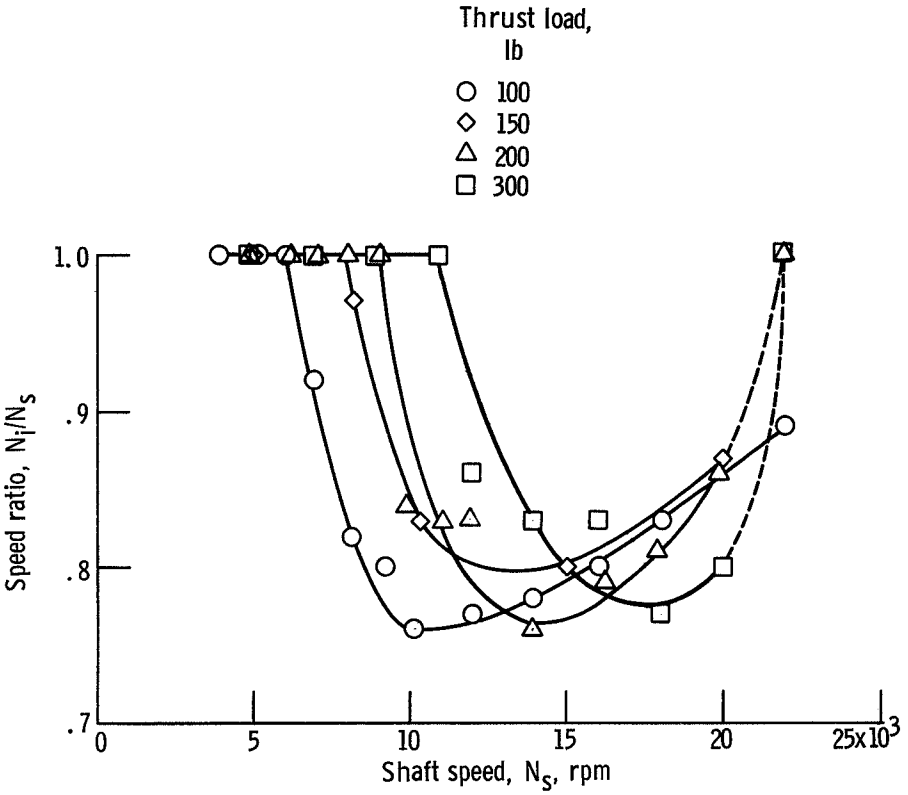

Figure 6. - Ratio of inner-race speed to shaft speed as function of shaft speed for original series-hybrid bearing.

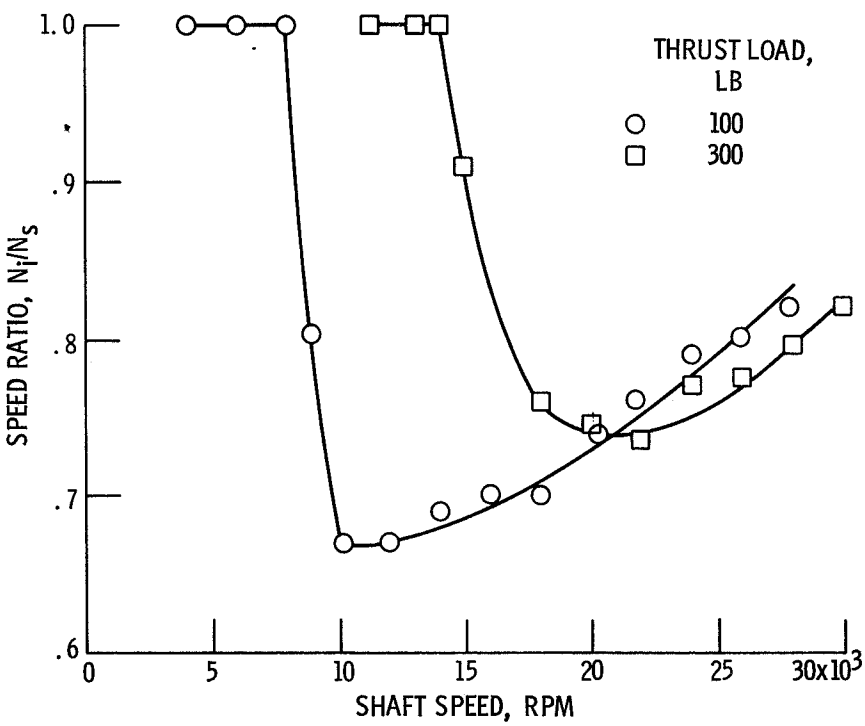

Figure 7. - Ratio of inner-race speed to shaft speed as function of shaft speed for modified series-hybrid bearing.

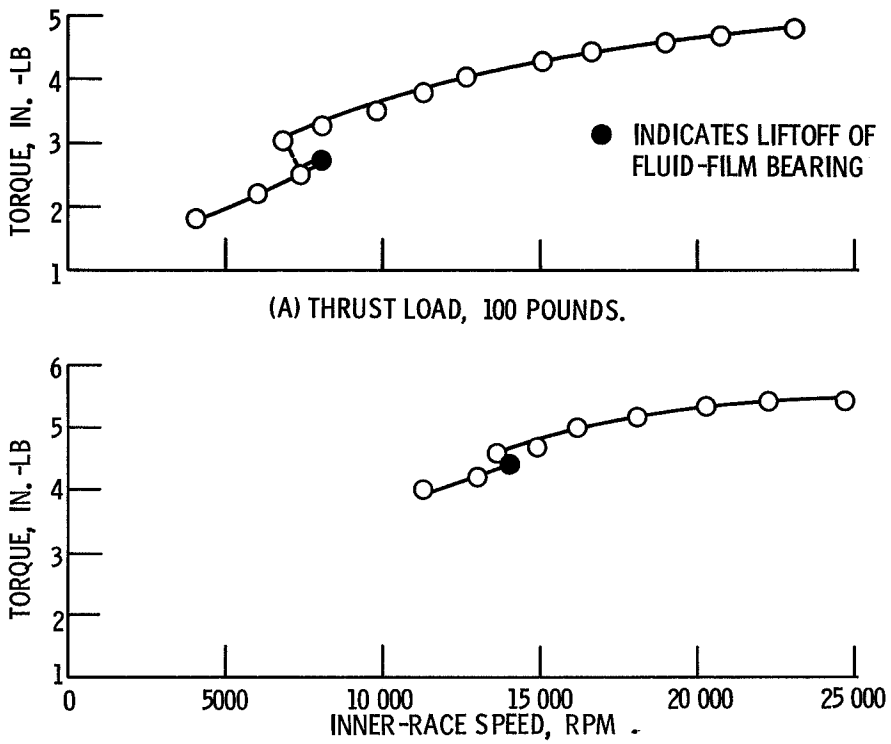

Figure 8. - Torque of modified series-hybrid bearing as function of inner-race speed.

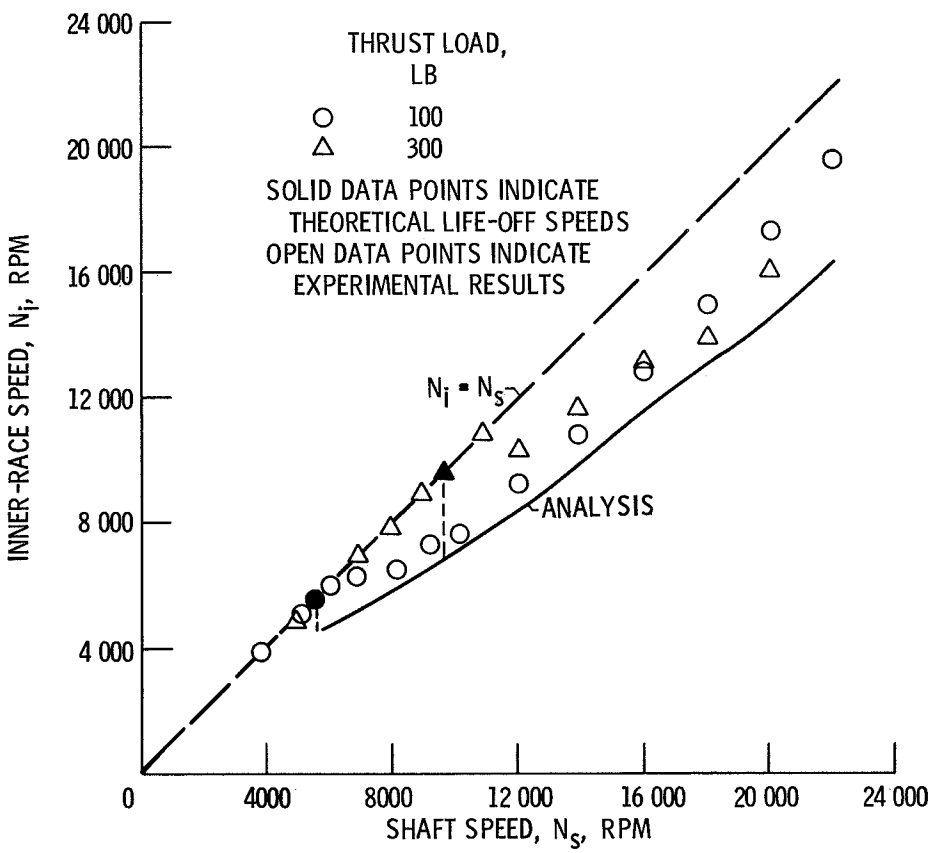

Figure 9. - Comparison of theoretical and experimental speed sharing results for original series-hybrid bearing.

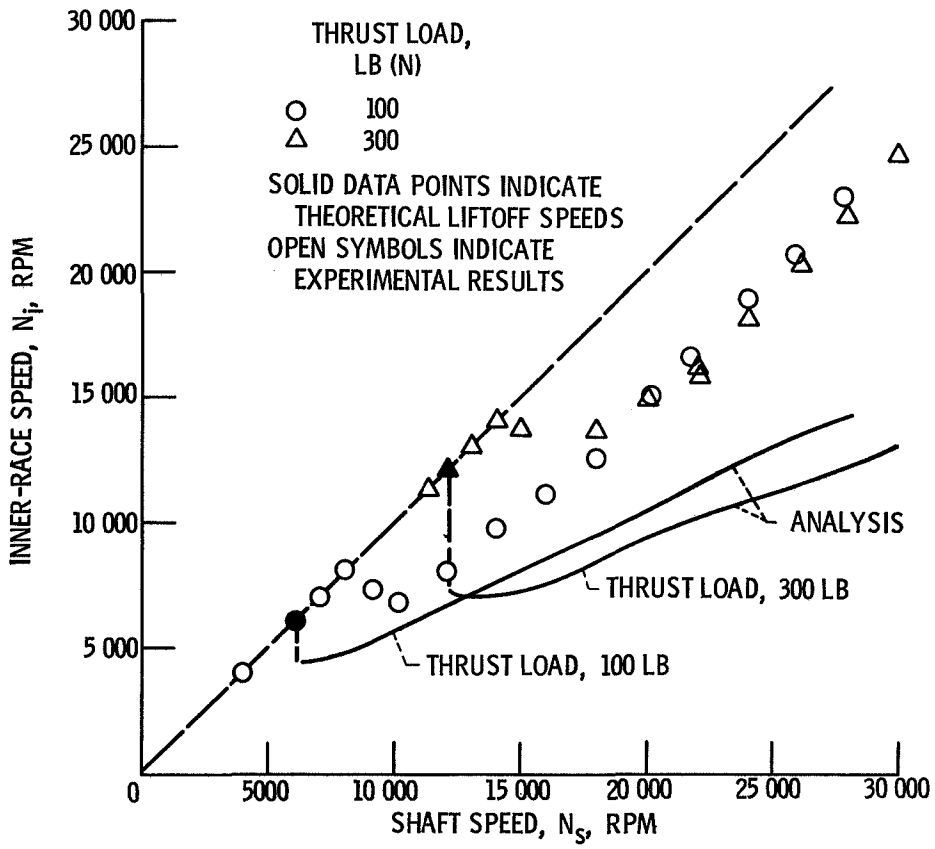

Figure 10. - Comparison of theoretical and experimental speed sharing results for modified series-hybrid bearing.